

Quasar 3C273

Optical Spectrum and Determination of the Redshift

Recorded with the DADOS Spectrograph
and the CCD Camera Atik 314L +

Richard Walker, CH-Rifferswil

richiwalker@bluewin.ch

Version 2.2 April 2019

Table of Contents

1	Introduction.....	3
2	Quasar 3C273	3
3	Key Data of 3C273.....	3
4	Identification and Properties of the Spectral Lines	4
5	Radial Velocities in the Vicinity of the Black Hole.....	6
6	The Redshift of the Spectral Profile.....	7
7	Estimation of the Apparent Recession Velocity	9
8	Estimation of the Distance applying the Hubble's Law	9
9	Estimation of the Distance applying Cosmological Models.....	9
10	Short Term Variations in the Spectral Profile of 3C273	10
11	Relative Radiometric Flux Correction of the Profile.....	10
12	Recording of the Spectrum – Considerations and Details.....	13
13	Bibliography and Internet Links	15

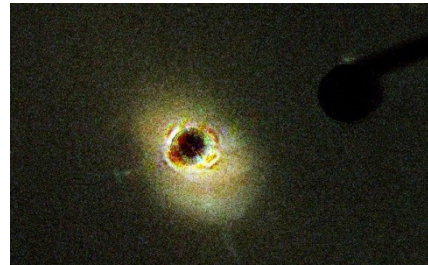
1 Introduction

The apparently brightest Quasar 3C273 in Virgo is often (wrongly) called the most distant object which can still be seen with average amateur means, purely visually and without the use of astronomical cameras. This document sets out which information can spectrographically be obtained - using a low-resolution slit spectrograph, enabling relatively short exposure times, and a cooled astronomical CCD camera of the younger generation.

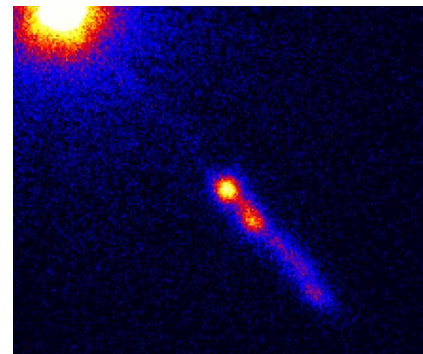
2 Quasar 3C273

The designation means the object number 273 in Ryle's third Cambridge catalogue of radio sources from 1959. The term "Quasar" is derived from *Quasistellar Object (QSO)*, because these objects appear as point shaped light sources. Maarten Schmidt discovered the first in 1963 at the coordinates of a corresponding entry in the mentioned radio source catalogue. It quickly became clear that this object showed the largest Redshift, known at that time, and therefore could impossibly be a star. In addition, the obtained spectra differed dramatically from stellar profiles and appeared more like those of Wolf Rayet stars, Nova outbursts, or even Supernova explosions.

According to today's knowledge, Quasars are considered as the most energetic and luminous version of active galaxies. The center of such an object always hosts a supermassive Black Hole which accumulates matter from the surrounding galaxy by an accretion disk. Therefore, Quasars are also strong sources of X-ray and radio emission. Their point shaped appearance can be explained by the enormous brightness of the nuclei, which in most cases totally outshine the rest of their host galaxies (HST image: 3C273). Apart from the episodically occurring Supernova explosions they are by far the most luminous objects in the universe.



The image of the X-ray satellite CHANDRA (source Wikipedia) shows a jet with a length of estimated 200,000 ly. It is generated by a part of the accretion flow, which is deflected in the direction of the Black Hole's rotation axis. Because Quasars are observed at very large distances only, we may see here an early stage of the galactic evolution. Even ordinary galaxies like the Milky Way host massive Black Holes in their central "bulge", which widely reduced the accretion process since a long time.



3 Key Data of 3C273

According to [1], [2], [5], [6]:

- Coordinates (epoch J2000): 12h 29' 06.7" +02° 03' 09"
- Redshift $z \approx 0.1583$
- Expansion of the space-time lattice ("escape velocity"): $c \cdot z \approx 47'469.1 \text{ km s}^{-1}$
- Apparent magnitude (slightly variable) $V \approx +12.7^m$
- Absolute magnitude: -26.7^M

The mass estimation of the Black Hole is still difficult and uncertain. The literature shows strongly scattering values for example [6], proposing a mass of some 1 Bn. M_{\odot} .

4 Identification and Properties of the Spectral Lines

Preliminary Remark: Despite the extreme Redshift of the spectrum, in this sect. 4 and in the following table, the spectral lines are discussed and displayed with their rest wavelengths λ_0 . The Redshift and its consequences are discussed later in sect. 6. The redshifted original scale was calibrated with a modified glowstarter bulb [26]. The scale of the *rest wavelength* was calibrated directly with the known λ_0 values at the very strong emissions of the H-Balmer series.

The identification of the spectral lines is chiefly based on [4], [5], [6], [7], [8]. The spectrum is dominated by extremely broadened emissions of the Balmer series and possibly by forbidden [O III] lines at $\lambda\lambda$ 5007 and 4959, fusing here to a blend. However the required, metastable initial states of such lines are extremely shock-sensitive, so they cannot arise in a turbulent environment and thus may appear at most marginally widened. Further it appears strange that this "[O III] emission" would show a much lower intensity, relative to H β . This observation would be in contrast to the spectral profiles of active Seyfert-type Galaxies, planetary nebulae and H II regions (see [23]). This phenomenon has already been noted by the discoverers of Quasars in the 1960ies.

Thus it is discussed whether the λ 5018 emission of the Fe II (42) multiplet ($\lambda\lambda$ 4923, 5018 and 5169) supplies the major contribution to the intensity of this emissions [4], [7]. This Trio frequently appears in the spectra of Active Galactic Nuclei (AGN), as well as in the profiles of Protostars, see [23].

Undisputed is the Ne III emission at λ 3869. The other features are mostly broad-band blends of different emissions, generated by various ions. This significantly complicates the line identification [7]. Consequently, their exact composition is still unclear. Striking is a broad emission between $\lambda\lambda$ 4500-4700. *J. B. Oke* [8] suggested as the cause the He II line at λ 4686 and numerous emissions of C III and N III - this in analogy with similar spectra of Supernovae and Wolf Rayet stars.

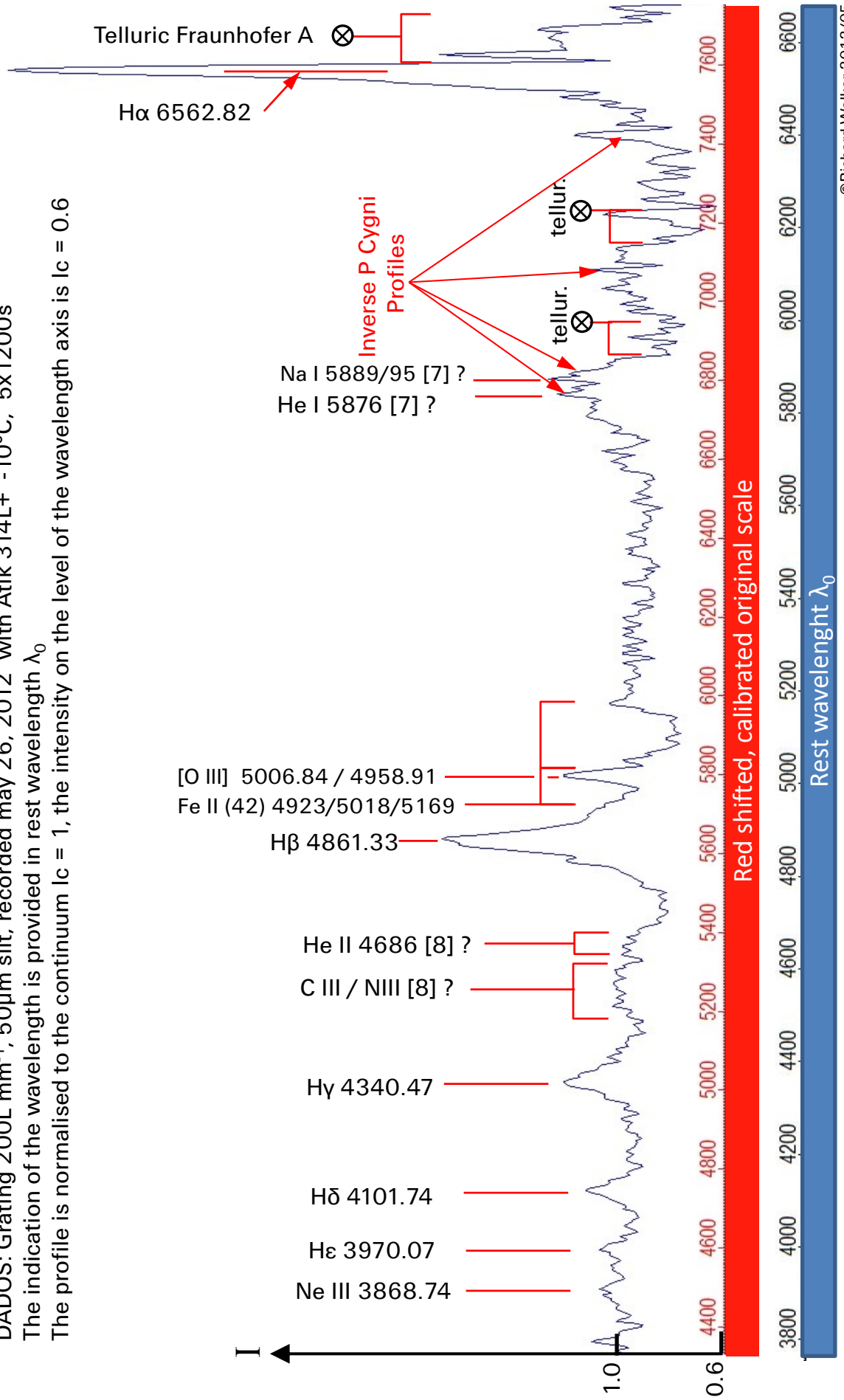
In [7] it is assumed that the striking emission in the range of λ 5870 is caused by He I at λ 5876. Under discussion is also the Na I doublet, which in certain phases can be observed during Nova eruptions. Due to the very low ionization energy of Na I these emissions must necessarily be generated at a considerable distance to the supermassive Black Hole. The same applies for the above mentioned shock sensitive [O III] lines.

An indication for the contraction process within the accretion disk are the inverse P Cygni profiles in the area around $\lambda\lambda$ 6100 - 6400, also observable in the spectra of the much smaller disks around the T Tauri and Ae/Be- Protostars [23].

The H α emission is redshifted so far that it coincides with the intense, telluric Fraunhofer A line. This is the cause why H α appears split here [8]. This circumstance complicates the determination of the Redshift, using this line (sect. 6), and seems at least to be one of the reasons for the very slow (flat) Balmer Decrement ($I_{H\alpha}/I_{H\beta} < 2.85$) [8] [22].

Quasar 3C273 Line Identification

DADOS: Grating 200L mm⁻¹, 50μm slit, recorded may 26, 2012 with Atik 314L+ -10°C, 5x1200s
 The indication of the wavelength is provided in rest wavelength λ_0
 The profile is normalised to the continuum $I_c = 1$, the intensity on the level of the wavelength axis is $I_c = 0.6$



5 Radial Velocities in the Vicinity of the Black Hole

The FWHM of the Doppler-broadened and Gauss fitted H β line enables a very rough estimation of the occurring radial velocity in the vicinity of the Black Hole [22]. Since the H α line appears split, this is done here at the Gaussfit the H β line. Due to the extreme line width the correction of the instrumental broadening is omitted here.

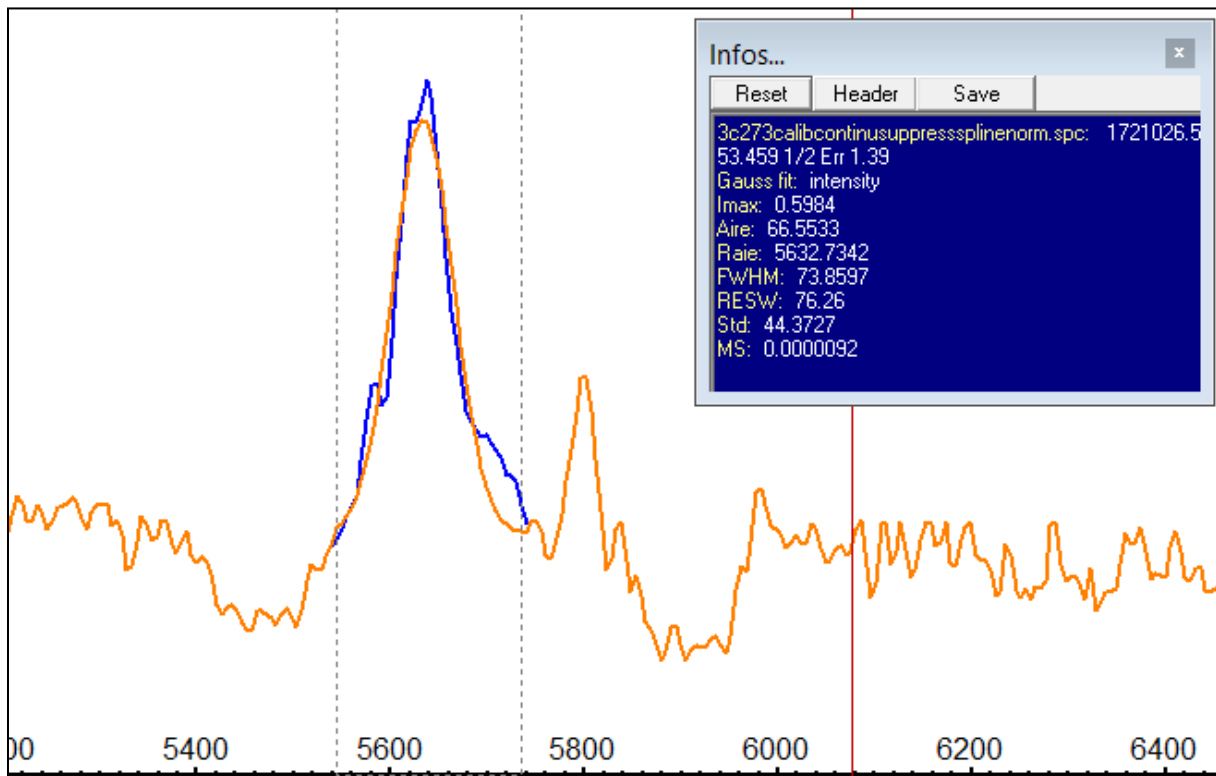
In this profile $FWHM_{Emission\ H\beta}$ results in 74 Å, whereas in contrast to [23], the range for the Gaussfit is restricted here to the upper part of the emission line and instead $\lambda_{0\ H\beta}$ the red-shifted value 5632 Å is applied.

The radial velocity of the matter, estimated with the Doppler principle results in:

$$v_r \approx \frac{FWHM_{Emission\ H\beta}}{\lambda_{0\ H\beta}} \cdot c \approx 4000\ km/s \quad \{1\}$$

This is roughly within the strongly scattering literature values and may yield different values, depending on the date and time of recording. For the jet however, based on X-ray analyses, up to 70% of the speed of light are postulated [3]. Of course this value cannot be measured with amateur equipment.

At the same time the Gaussfit (brown line) determines here the redshifted wavelength of the H β Balmer line ("Raie")



6 The Redshift of the Spectral Profile

Preliminary remark: In this section 6 and on the following table, redshifted wavelengths are indicated, measured at Gaussian fitted lines and related to the original wavelength scale, calibrated with a modified Glowstarter bulb [26]. The apparent "escape-" or radial velocity v_r is calculated here with the classical spectroscopic Doppler formula [22].

$$v_r = \frac{\Delta\lambda}{\lambda_0} \cdot c \quad \{2\} \qquad \Delta\lambda = \frac{v_r \cdot \lambda_0}{c} \quad \{3\}$$

If formula {2} is converted for the explicit calculation of the Redshift $\Delta\lambda$ {3}, we can recognize, that for a given radial velocity, the amount of the shift $\Delta\lambda$ is proportional to the rest wavelength λ_0 of the corresponding spectral line. This can impressively be seen in the spectrum of 3C273. While the H α line, with the rest wavelength of 6563Å, is shifted by the huge amount of about 1017Å to $\sim\lambda$ 7580Å (!), the Redshift of the H δ line amounts here to just 646Å.

In the field of astrophysics for such highly red shifted objects, the distance is usually expressed directly as z -value. It can easily be determined by the measured Redshift in the spectrum and is independent of assumptions for cosmological model parameters (eg Ω). Due to the constant speed of light c , z is also used as a measure of time for the past.

$$z = \frac{\Delta\lambda}{\lambda_0} \quad \{4\}$$

For reasons of proportionality the dimensionless z - values remain independent from the wavelength of the analyzed line. In the following table they are listed for all H-Balmer lines in the profile of 3C273, with the exception of the split H α emission. A heliocentric correction is omitted here, because the apparent "recess velocity" reaches almost 20% of the speed of light!

Line	$\lambda_{redshifted}$ (*)	λ_0	$\Delta\lambda$	z
H β	5632	4861	771	0.1586
H γ	5023	4340	683	0.1574
H δ	4748	4102	646	0.1574

(*) measured with Vspec at Gaussian fitted lines

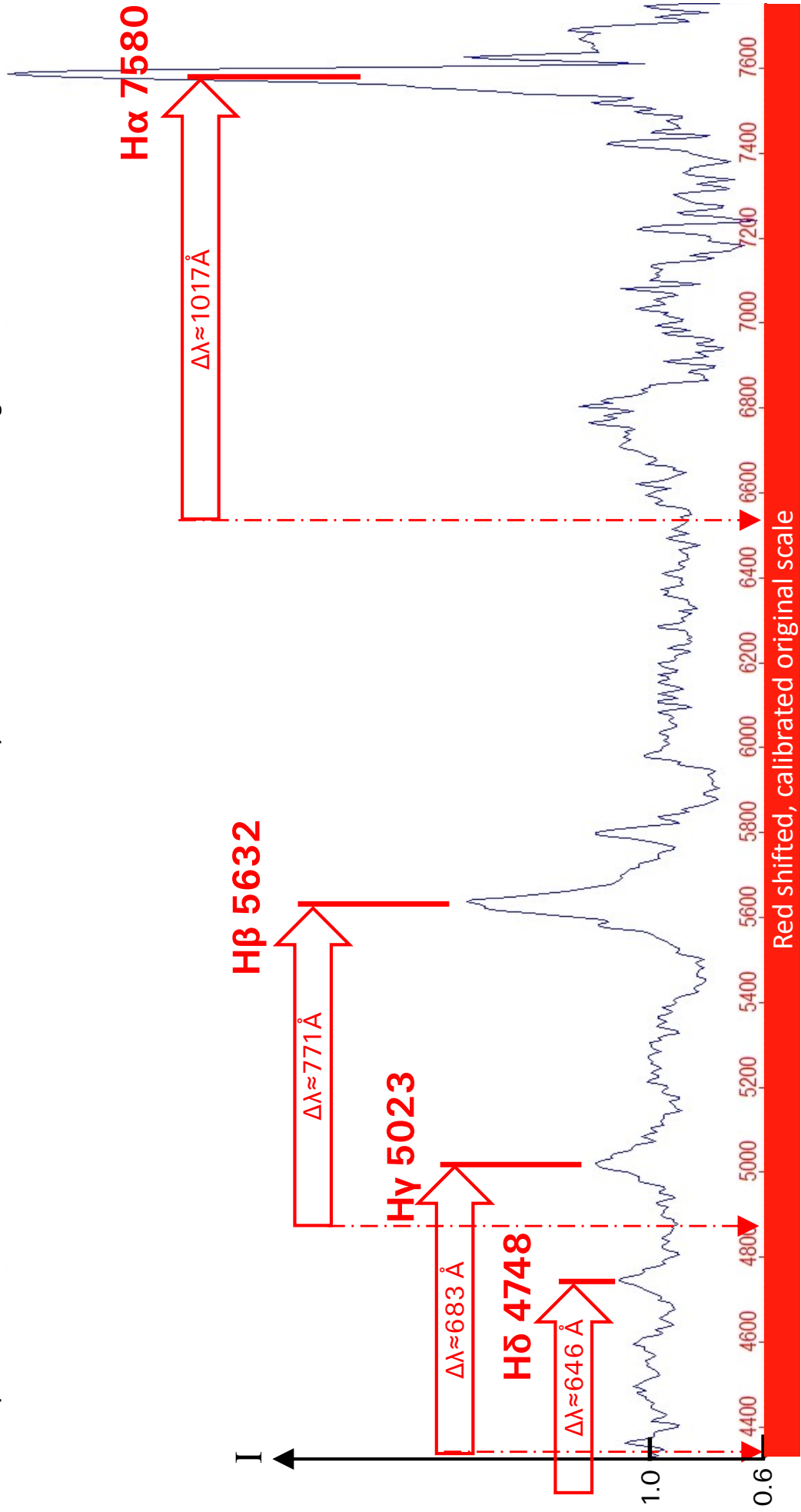
According to [1] and [2] the accepted value is $z \approx 0.1583$. Thus the present measurements are consistent here up to almost three decimal places.

There exist Quasars with Redshifts up to $z > 10$. Accordingly in the literature one can find spectral lines in the optical part of the profile, which under normal conditions are located in the UV region of the spectrum, such as L α of the Lyman series. Therefore, it becomes understandable why, among other reasons, current and future space telescopes will be increasingly optimized for the infrared range of the spectrum.

Quasar 3C273, Redshift of the Hydrogen Balmer Lines

DADOS: Grating 200L mm⁻¹, 50µm slit, recorded may 26, 2012 with Atik 314L+ -10°C, 5x1200s

The indication of the wavelength, determined with Vspec at Gaussfits, is provided red shifted on the original scale. The profile is normalised to the continuum $I_c = 1$, the intensity on the level of the wavelength axis is $I_c = 0.6$.



7 Estimation of the Apparent Recession Velocity

With the known z value we can estimate now the apparent recession velocity. "Apparent" means that the object is not cinematically moving away from us, but the space in between or the so-called "space-time lattice" is expanding [10]. Consensus seems to prevail here amongst the cosmologists. By combining the formulas {2} and {4} we get:

$$v_f = c \cdot z \quad \{5\}$$

Thus for 3C273 we get $v_f \approx 47'490 \text{ km s}^{-1}$. By contrast, the z and v_f values of the Messier galaxy world are comparatively modest. Record holder here is M88 with $z = 0.0076$ corresponding to $v_f \approx 2281 \text{ km s}^{-1}$ [22].

In formula {5}, however, it becomes immediately obvious that at values from $z > 1$ we get $v_f > c$ and thus an apparent dilemma arises. In the past in this case the modified Doppler formula, taking into account the effects of the Special Theory of Relativity SRT, was sometimes used as a way out [9], [22].

$$v_r = c \cdot \frac{(z + 1)^2 - 1}{(z + 1)^2 + 1} \quad \{6\}$$

Today, this is rejected by most experts and instead cosmological models are applied, based on the General Theory of Relativity ART (chapter 9).

8 Estimation of the Distance applying the Hubble's Law

The classical method to estimate the distance D is based here on the Hubble's law [22].

$$v_f \approx c \cdot z \approx H_{(0)} \cdot D \quad \{7\} \quad \text{Hubble Constant } H_{(0)} \approx 73 \text{ km s}^{-1} \text{ Mpc}^{-1}$$

By converting of formula {7} we get the distance D in [Mpc]

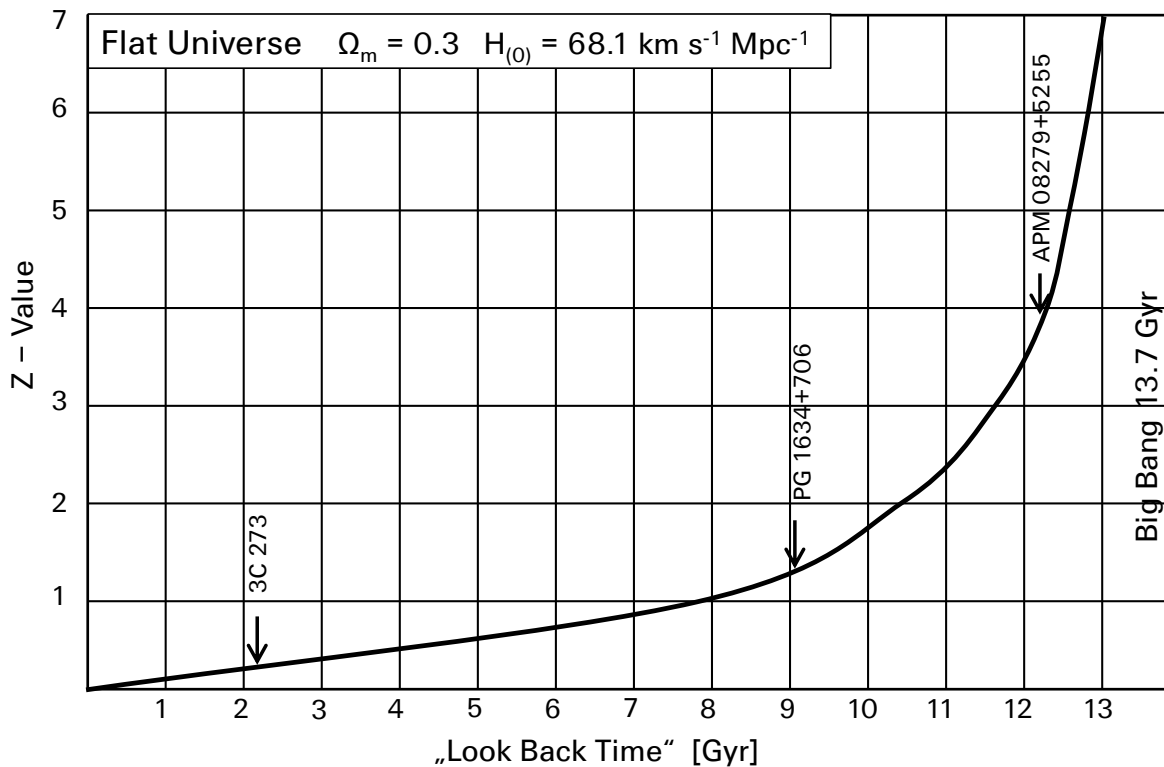
$$D \approx \frac{c \cdot z}{H_{(0)}} \quad \{8\}$$

Formula {8} also expresses that the distance D increases proportional to the Redshift z . However, this proportionality of the Hubble law remains acceptable only up to about $z \approx 0.1$ (about 400 Mpc). For higher z -values, appropriately parameterized cosmological models must be used [10]. Nevertheless, if the Hubble law is applied conventionally to 3C273, it results a distance D of approximately 650 Mpc or 2.12 billion ly.

9 Estimation of the Distance applying Cosmological Models

For the estimation of distances with high z -values cosmological models exist, which can also be applied by amateurs. Thanks to technological advances we can now penetrate into cosmologically relevant distance ranges up to $z \approx 4$. So we must be aware of the effects of the ART and of the still-debated cosmological models. For this purpose there exist various programs [12] [13] [14], mostly just requiring the input of the components for the cosmological density parameters Ω_m and Ω_Λ and the Hubble constant $H_{(0)}$. Currently, widely accepted, is a flat, Euclidean universe with $\Omega_m + \Omega_\Lambda \approx 1$ ($\Omega_m = 0.3$, $\Omega_\Lambda = 0.7$) and a Hubble Constant, within a range of about $67 - 73 \text{ km s}^{-1} \text{ Mpc}^{-1}$ (for details see [22]).

Mostly based on these parameters, such tools allow the calculation of single values or even the plotting of diagrams, representing e.g. the distance as a so-called "look back time" in a function of the measured z -value. The following diagram was generated with the "Cosmologic Calculator II" by Nick Gnedin of the University of Chicago and based on the suggested default values [12]. Indicated on the curve are some particularly bright quasars which today can spectroscopically be recorded, even by amateurs with appropriate instruments and sufficiently large apertures.



10 Short Term Variations in the Spectral Profile of 3C273

The table on page 11 shows a montage of two profiles. They have been recorded within only 12 days and are normalised on the same section to $I_c = 1$. In the first profile, recorded May 14, 2012, the H α line is missing, because by the initial setting of the wavelength range the expected massive Redshift has been simply forgotten. The hydrogen Balmer lines and the O III emission of the two profiles appear not significantly different. However, striking in the profile of May 14, 2012 is the highly elevated “bump” in the range of about 7000Å, which is still superposed by an emission of unknown origin. Another difference is noted in the area around 6100 Å.

The example shows impressively that significant variations can occur in this spectrum within a relatively small period of time. It also shows that this central region can't be indefinitely large, and according to www.hubblesite.org can therefore hardly exceed the diameter of our solar system. 3C273 would certainly be a highly interesting candidate for a monitoring project.

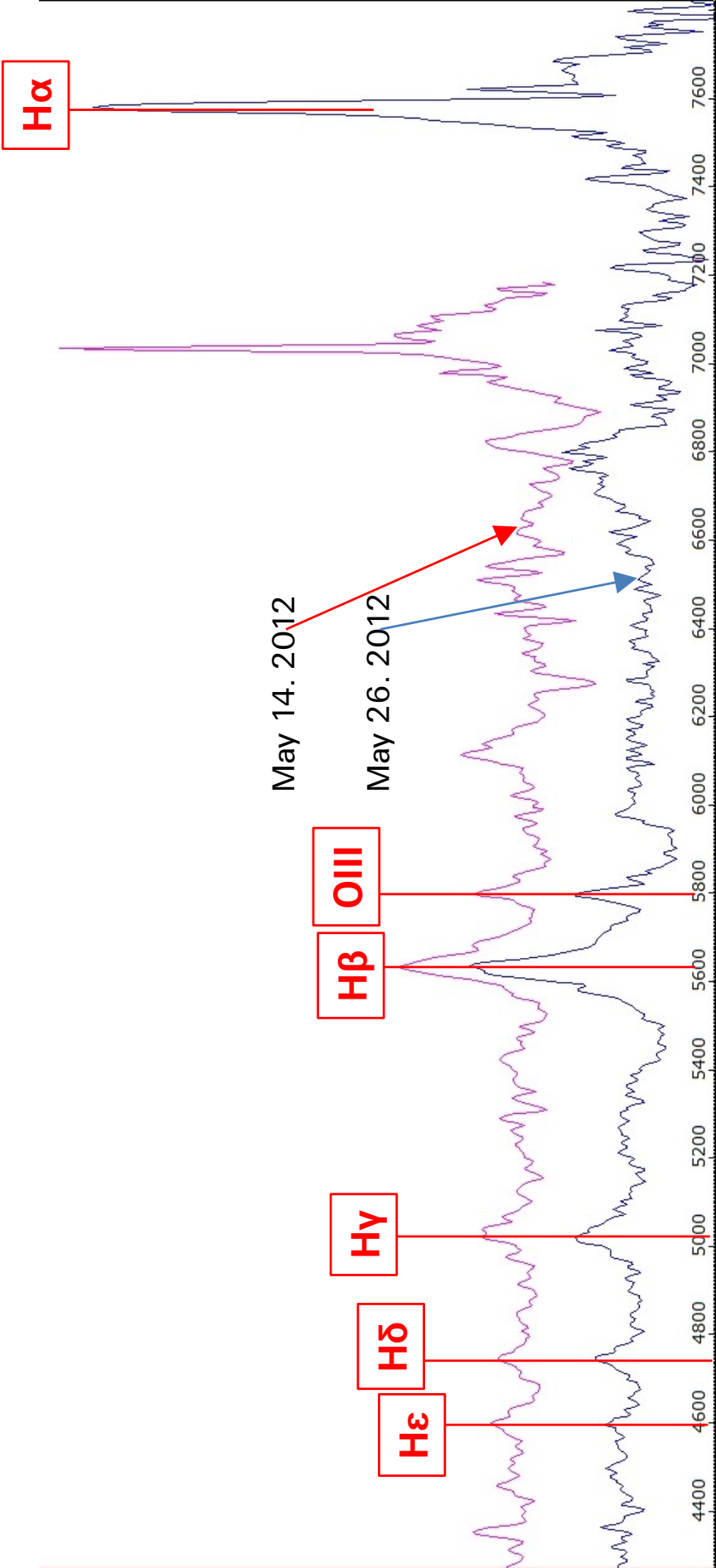
Important: In addition to such considerations we should always be aware that these changes, observed within a very short time, took place about 2.4 billion years ago, when our earth was still in the Precambrian geological age!

11 Relative Radiometric Flux Correction of the Profile

The table on page 12 is just intended to provide a rough, qualitative impression of the relative flux of the Quasar continuum. Alternatively to a calibration of the spectral flux density by a recorded standard star [22], this calibration curve was generated here with the synthetic standard profile of a O5 type star in the Vspec Library, because also Quasars radiate excessively in the UV and X-ray range.

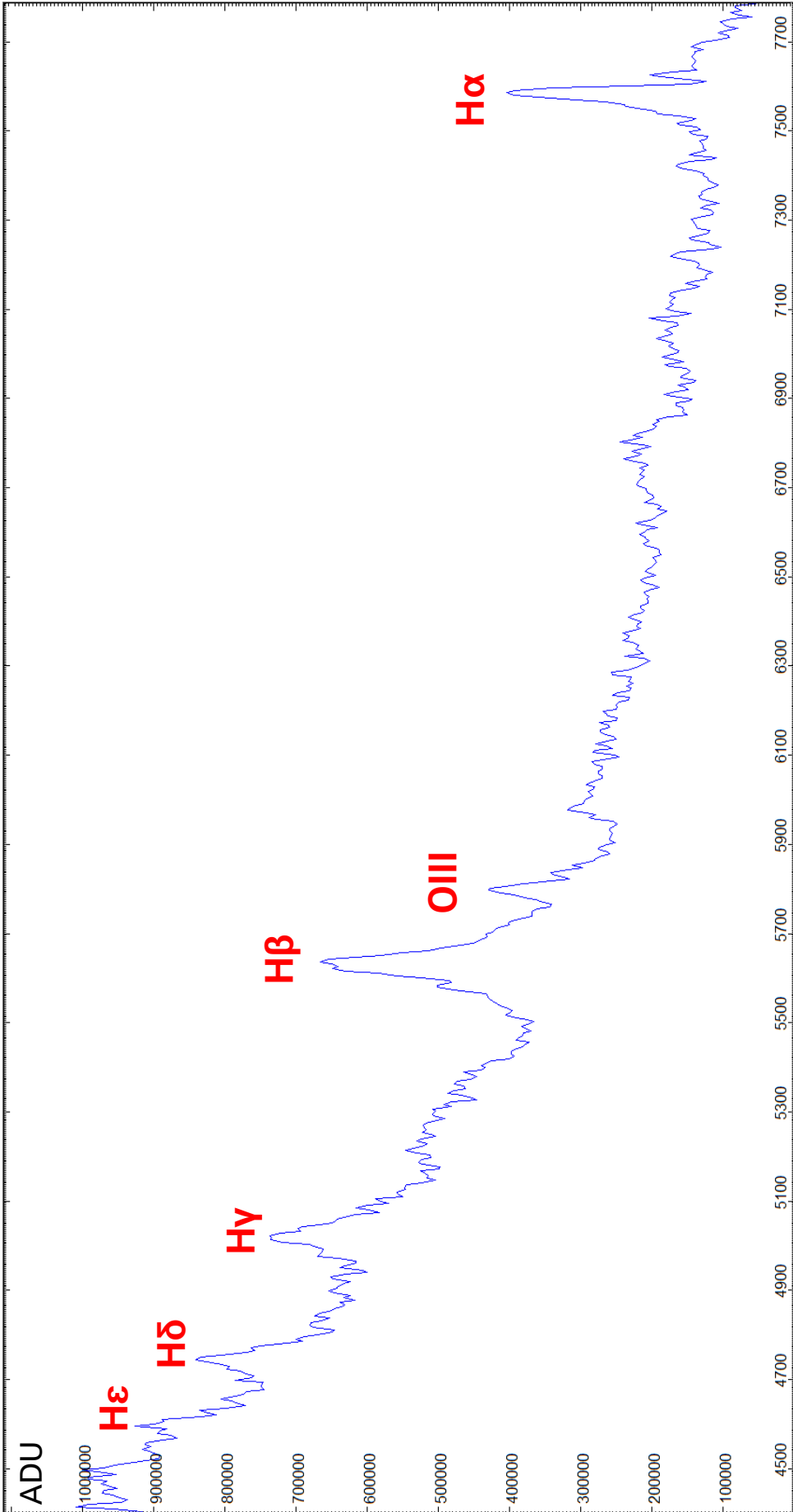
Quasar 3C273 Variations in the Spectral Profile

DADOS: Grating 200L mm⁻¹, 50µm slit, recorded may 14, and 26, 2012 with Atik 314L+ -10°C, 5x1200s
The indication of the wavelength corresponds here to the original red shifted scale
The superposed profiles are normalised to the continuum I_c = 1 and shifted in parallel by an integer



Quasar 3C273 Profile with Relative Radiometric Flux-Correction

DADOS: Grating 200L mm⁻¹, 50μm slit, recorded may 26, 2012 with Atik 314L+ -10°C, 5x1200s
The indication of the wavelength is provided red shifted on the original scale. The intensity scale shows ADU.
The profile is relatively Flux-corrected, based on a correction curve, generated with a synthetic O5 Standard star (Vspect).



Red shifted, calibrated original scale

12 Recording of the Spectrum – Considerations and Details

Up to now such faint objects were generally regarded as the domain of the (slitless used) transmission grid. This is shown by numerous examples of 3C273 as well as of extragalactic Supernovae, recorded by amateurs.

However, recordings of even much fainter objects in the spectral atlas have shown that in principle all objects, which are just barely visible on the split mirror, can be recorded spectroscopically with accordingly long exposure times [22], [23]. Therefore 3C273 with $\approx 12.7^m$ does not represent the magnitude limit of a C8 Telescope and for larger apertures, more quasars, with a slightly lower brightness, get within a realistic range. The DADOS Manual of 2008 estimated the magnitude limit still at about 8^m , at that time based on 30cm aperture, an exposure time of 20 minutes and $9\mu\text{m}$ pixel size!

The quasi-stellar, punctiform appearance of the Quasar considerably facilitates the recording of the spectrum. The nebula of the very faint Supernova remnant M1 was much more difficult and required a minimum of 30 minutes per single shot. With the C8, the 200L mm^{-1} grating and the Atik 314L+, cooled to -10°C and applied in 2x2 binning mode, 20 minutes exposure time have been proven as sufficient. The result is a somewhat noisy profile but would already allow a rough determination of the Redshift. The stacking of several such profiles already reveals fine structures and allows the determination of the Redshift with an accuracy of nearly three decimal places. For high quality astrophotography mostly much more exposure time must be applied!

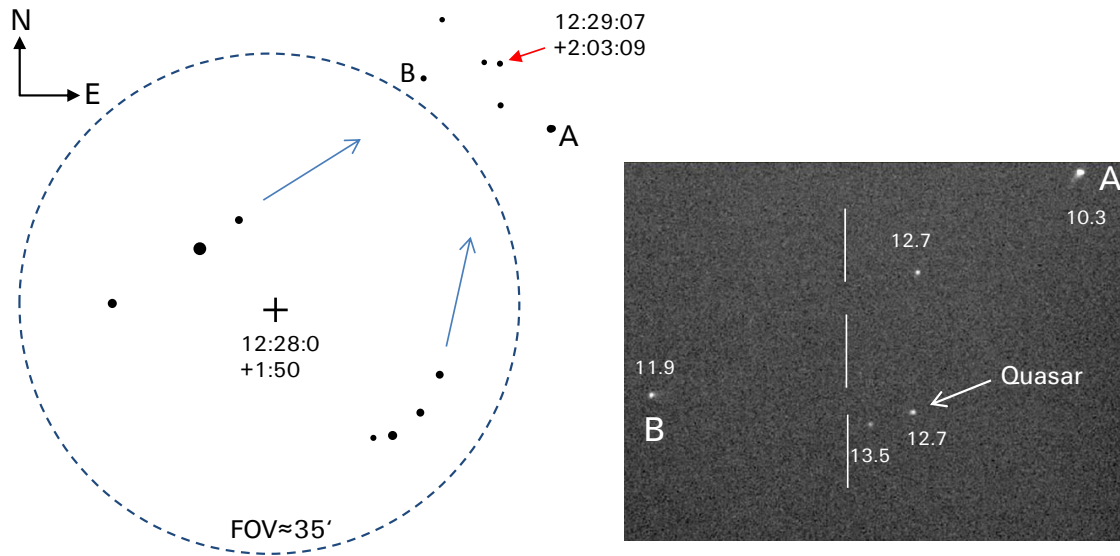
Due to the small pixel size of $6.45\mu\text{m}$, the application of the 2x2 binning mode barely impairs here the resolution, even not with the smallest $25\mu\text{m}$ slit [22]. However the required exposure time is considerably more than halved thereby. At fainter objects, applying the $50\mu\text{m}$ slit, even the 3x3 binning mode could be used with a moderate loss of resolution.

With such long exposure times in our densely populated areas, the light pollution artefacts must be subtracted from the recorded spectrum [22]. For point light sources and long slits this can directly be done together with the sky background and based on the same spectral image.

The PHD autoguiding was performed with the DSI II slit camera on a neighbouring faint star. The C8 was mounted on a Vixen Sphinx SXD Deluxe. An exposure time of 3.5s has been applied for the guiding camera. Anyway a very clear sky is required without any thin cirrus clouds.

To facilitate the orientation, finally a finding chart is attached. The blue circle on the left shows the field of view (FOV) observed with a 25mm eyepiece on a flip mirror, mounted between the telescope (C8) and spectrograph. Within the circle two distinct rows of stars can be seen. They serve here as "pointer stars" to the faint star group, which hosts 3C273. Star **A** is there by far the brightest with 10.3^m .

The indicated magnitudes are based on AAVSO enabling a rough estimation of the "current" luminosity of 3C273. The object of course can also directly be approached to its coordinates by applying the GOTO function of the telescope mount. The screenshot at right shows the apparent Quasar environment, appearing on the PHD Guiding screen accordingly mirrored, taken with the chosen orientation of my DSI II slit camera. The star, directly adjacent to 3C273, is slightly weaker with some 13.5^m .



13 Bibliography and Internet Links

Database:

[1] CDS Strassbourg: *SIMBAD Astronomical Database* with the most important data about astronomical objects like fixed stars, galaxies, star clusters etc. <http://simbad.u-strasbg.fr/simbad/>

[2] *NASA Extragalactic Database (NED)* with the most important data, spectra, images etc. to galaxies and Quasars <http://nedwww.ipac.caltech.edu/>

Literature und Links:

[3] M. J. Avara, *Precision X-Ray Spectroscopy of 3C273 Jet Knots*, MIT 2008
<http://dspace.mit.edu/bitstream/handle/1721.1/44464/297176629.pdf?sequence=1>

[4] B.M. Peterson et al. *Are Forbidden Lines Present in the Optical Spectrum of the QSO 3C 273?* Ohio State University 1984 <http://articles.adsabs.harvard.edu/full/1984ApJ...283..529P>

[5] B.M. Peterson et al. *Central Masses and Broad-Line Region Sizes of Active Galactic Nuclei. II. A Homogeneous Analysis of a Large Reverberation-Mapping Database.* The Astrophysical Journal 2004 <http://arxiv.org/abs/astro-ph/0407299>

[6] S. Paltani, M. Türlér: *The mass of the black hole in 3C273*, 2005 Marseille, Geneva
<http://arxiv.org/abs/astro-ph/0502296>

[7] A. Boksenberg et al. *New Spectrometric Results on the Quasar 3C273*, University London 1974
<http://adsabs.harvard.edu/full/1975MNRAS.172..289B>

[8] J.B. Oke: *The Optical Spectrum of 3C273*, CALTECH 1964
<http://adsabs.harvard.edu/abs/1965ApJ...141....6O>

[9] Fritz Kurt Kneubühl, *Repetitorium der Physik*, Teubner Studienbücher Physik, Kap. *Relativistischer Doppler-Effekt der elektromagnetischen Wellen*

[10] Lexikon Astronomie Wissen, Andreas Müller, TU München
<http://www.wissenschaft-online.de/astrowissen/>

[11] Christian Buil: *Observations avec le Spectrographe Lisa*
<http://www.astrosurf.com/buil/lisa6/obs.htm>

[12] Nick Gnedin: *Cosmological Calculator for the Flat Universe*
<https://home.fnal.gov/~gnedin/cc/>

[13] Alberto Cappi: *COSMOTOOLS V1.0*, INAF Osservatorio Astronomico di Bologna
<http://www.bo.astro.it/~cappi/cosmotools>

[14] Cosmological Calculator, Feb 2013 (LCDM model, default inputs: Planck mission 2013)
http://www.einsteins-theory-of-relativity-4engineers.com/cosmocalc_2013.htm

Author:

[22] Marc Trypsteen, Richard Walker: *Spectroscopy for Amateur Astronomers - Recording, Processing, Analysis and Interpretation*, 2017 Cambridge University Press, ISBN: 9781107166189

[23] Richard Walker: *Spectral Atlas for Amateur Astronomers - A Guide to the Spectra of Astronomical Objects and Terrestrial Light Sources*, 2017 Cambridge University Press, ISBN: 9781107165908

The following scripts on the subject (some of them in German) are downloadable under this link:
<http://www.ursusmajor.ch/astrospektroskopie/richard-walkers-page/index.html>

[24] *Spectral Data Reduction for Amateur Astronomers, Task-oriented Tutorial with Freeware Programs*

[25] *Atomic Emission Spectroscopy with Spark- or Arc Excitation, Experiments with the DADOS Spectrograph and Simple Makeshift Tools*

[26] *Glow Starter RELCO SC480, Atlas of Emission Lines*